Tm3+ codoping for mid-infrared laser applications of Dy3+ doped CaF2 crystals

Gurvan Brasse, Rémi Soulard, Jean-Louis Doualan, A. Braud, Abdelmjid Benayad, Patrice Camy

Version of Record: https://www.sciencedirect.com/science/article/pii/S0022231320318196
Manuscript_1f13ac3801f277bcf73ed4c6ec633bba

Tm^{3+} codoping for mid-infrared laser applications of Dy^{3+} doped CaF_2 crystals

Gurvan BRASSE[1], Rémi SOULARD[2], Jean-Louis DOUALAN[1], Alain BRAUD[1], Abdelmjid BENAYAD[1] and Patrice CAMY[1]

[1] *CIMAP – Centre de recherche sur les Ions, les Matériaux et la Photonique - UMR 6252 CEA-CNRS-ENSICAEN- Normandie Université, 6 Boulevard du Maréchal Juin - 14050 CAEN Cedex 4 - FRANCE*

[2] *Laboratoire ARTEMIS, UMR 7250 Université Côte d'Azur-CNRS-Observatoire de la Côte d'Azur, F-06304 Nice, FRANCE*

Abstract

We report here on a spectroscopic study of Dy^{3+}-doped and Tm^{3+}-Dy^{3+} doped CaF_2 as promising candidates to develop crystalline waveguide laser sources around 3 µm. The advantages of Tm^{3+} ions as sensitizers to improve the excitation of Dy^{3+} ions in CaF_2 is demonstrated: an energy transfer efficiency from Tm^{3+} to Dy^{3+} ions of 99.6% has been reached for Dy^{3+} concentration as high as 2 at.%, by considering a Tm^{3+} ratio set at 5 at.%. Moreover, the behavior of such doped crystals in a laser waveguide configuration has been modeled and the modeling results show that it seems possible to achieve promising laser perspectives around 3 µm, with laser thresholds in the watt level for singly doped Dy^{3+}:CaF_2 and around 0.2-0.3 W for codoped Tm^{3+}-Dy^{3+}:CaF_2, presenting both laser efficiencies in the order of 30%. Finally, the saturation of the absorption which is observed in the modeling for such codoped Tm^{3+}-Dy^{3+}:CaF_2 waveguide at Dy^{3+} concentration below 1% is discussed and its origin is explained.

Keywords: Mid-Infrared, Laser, Spectroscopy, Dysprosium, Calcium Fluoride, Waveguide

1. Introduction

Mid-infrared (MIR) coherent light sources are of great interest for numerous applications ranging from spectroscopy [1], biomedicine and surgery [2], material processing [3], defense and security [4]. This comes from the fact that this spectral range contains the spectroscopic signatures of most basic molecules vibrations [1]. Up to now, very few laser media provide an efficient laser emission in the 2-4 µm spectral range and the development of laser sources in this spectral window appears as a major and international challenge for cutting edge applications [1] [2][3]. Indeed, there is a renewed interest for the development of such MIR materials, especially for their implementation in high-power ultrafast lasers and amplifiers operating in the Near-Mid-Infrared (Near-MIR) around 3 µm. Such laser capabilities would open the way towards the development of novel supercontinuum sources extending further in the mid-IR [5] and would constitute very exciting tools for frequency combs [6] and high order harmonics generation (HHG) [7,8] that will be extremely useful for attoscience [9] and strong fields physics applications [10].

Dysprosium doped fluoride crystals appear to be very relevant candidates to develop laser sources around 3 µm, because of the Dy^{3+} $^6H_{13/2} \rightarrow {}^6H_{15/2}$ radiative transition and the fluoride relatively low

maximum phonon energy (< 500 cm^{-1}), that reduces rare earth non-radiative relaxations processes and enables radiative transitions in the Mid-Infrared spectral range. Guggenheim and Johnson have demonstrated for the first time the stimulated emission at 3.022 µm of Dy^{3+} doped BaY_2F_8 (Dy^{3+}: BYF), under flash lamp pumping [11]. Few years later, Antipenko *et al* have reported the stimulated emission of Dy-doped LaF_3 under a pulsed pumping at 1.06 µm [12]. More recently the 3.4 µm laser emission of Dy^{3+}-doped $BaYb_2F_8$ has been obtained at room temperature under pulsed laser pumping at 1.3 µm [13], while CW laser emissions in the range [2.8 - 3.4 µm] has been achieved in Dy^{3+}-doped ZBLAN optical fibers [14][15][16][7][18], as well as in glassy InF_3 optical fibers [19].

Laser oscillation around 3 µm can be achieved in Dy^{3+} doped fluoride hosts by pumping at 2.8 µm, 1.7 µm, 1.3 µm or 1.1 µm, as it has been demonstrated in previous studies. Nevertheless, these pump wavelengths do not correspond to any commercially available high power laser diodes, which is a real drawback to develop compact and low cost laser systems. Dy^{3+} ions can also be pumped around 800 nm and 900 nm, which facilitate pumping with existing pump sources, but induce a significant quantum defect and a less efficient absorption of the pump. The alternative route proposed in this work to overcome these limitations is to use Tm^{3+} ions as sensitizers that can be easily pumped around 770 nm, with high power laser diodes.

Previous works have studied the effect of Tm^{3+} codoping in Dy^{3+} doped fluoride crystalline host matrices like BaY_2F_8, KY_3F_{10}, $LiYF_4$ [20][21] and more recently LaF_3 [22], but such a study has never been reported in Dy^{3+} doped and Tm^{3+}-Dy^{3+} doped CaF_2. Indeed, CaF_2 is an interesting host matrix which present good thermo-mechanical properties, as well as a broad transparency window from 0.2 µm until 6-7 µm. Moreover, CaF_2 has already proven its relevance as a first choice laser material, especially for laser application at 1 µm [23], but also more recently around 2 µm in a CW-regime [24][25], as well as in pulsed regime [26] [27]. Furthermore, CaF_2 is used today in high power laser chains, as well as in various commercial laser devices and presents the required characteristics to become a first choice material for laser emission around 3 µm. When the rare earth doping level in CaF_2 excess 0.1%at, a clustering effect takes place [28]. So, in the case of a codoping with Tm^{3+}-Dy^{3+} ions, a well known cross relaxation process between Tm^{3+} neighboring ions and an efficient energy transfer from Tm^{3+}($^3F_4$) to Dy^{3+}($^6H_{11/2}$) ions occur, allowing thus an efficient emission of Dy^{3+} ions around 3 µm and a reduction of the quantum defect. In addition, it is also known that this clustering effect, which is observed in CaF_2, induces a broadening of the absorption and emission bands that appear as a strong advantage to achieve short pulse laser operations for high power applications [25]. Otherwise, other works have also studied the effect of Tm^{3+} codoping in Dy^{3+} doped oxide crystals like $YAlO_3$ [29] and similar detailed spectroscopic studies have been carried out on various Dy^{3+} doped and Tm^{3+}-Dy^{3+} doped glasses based on chalcogenides like $Ge_{25}Ga_5S_{70}$ [30,31], chalcohalides [32,33], fluorophosphate [34], as well as on fluorides glasses [35]. Nevertheless, CaF_2 crystals allow a better management of the thermal effects than glassy materials, which is particularly important for a power rise.

This article present, for the first time to our knowledges, a thorough spectroscopic study of the Dy^{3+} and Tm^{3+}-Dy^{3+} doped CaF_2 crystals. The advantages of Tm^{3+} codoping for such a system is highlighted and an original modeling of the laser potential around 3 µm of such Dy^{3+} and Tm^{3+}-Dy^{3+} doped CaF_2 crystal is proposed and discussed for a microstructured channel waveguide configuration. Although the spectroscopy of various materials codoped with Tm^{3+} and Dy^{3+} ions have been studied in the considered spectral range, over the last 20 years, no lasing around 3 µm according to this scheme have been demonstrated. This could be explained by the fact that these laser experiments have been essentially carried out on bulk materials, whereas relevant and promising results have been demonstrated on singly Dy^{3+} doped fluorides optical fibers at the same time [14][15] [16][17][18], so that the efforts may have been focused on this approach without the need of Tm^{3+} codoping. Nevertheless, the glassy nature of such optical fibers present some limitations which are difficult to manage when the pump power increase, especially the thermal and non-linear effects. Today, another approach to get laser emission of

Dy^{3+} around 3 µm can be considered, as an interesting compromise between bulk crystals and glassy optical fibers: it is the microstructured waveguide configuration which is based on high optical grade Tm^{3+}-Dy^{3+} doped single crystalline CaF_2 epitaxial layers that can be grown by liquid phase epitaxy (LPE) [36]. Indeed, the technology to achieve high optical grade crystalline epitaxial layers of fluorides was not mature enough 20 years ago. Nowadays, it is possible to realize such microstructured waveguides presenting low optical losses, which can be associated to the new pumping capabilities. Such an approach can indeed associate the advantages of a strong confinement of the laser beam in the guiding medium, as well as the length of this gain medium that can be centimeters long, hence the interest of the modeling, which is proposed after the spectroscopic study in this article.

2. Materials and experimental details

2.1 Crystals growth and preparation

The Dy^{3+}-doped CaF_2 and Tm^{3+}-Dy^{3+} doped CaF_2 single crystals are synthesized by using the Bridgman technique. Briefly, the principle of this technique consists in translating vertically a crucible full of molten raw materials through the thermal gradient of a furnace: the crucible moving from the higher temperatures to the lower temperatures allows the crystallization on a seed and the propagation of the growth front throughout the whole molten mixture. The melting temperature of CaF_2 and consequently its crystallization temperature, lies around 1450°C. The following rare-earth doping in at. %, have been studied in CaF_2: CaF_2:X%Dy^{3+} for X = 0.1 - 0.2 - 0.5 - 1 - 2 - 3 - 5 and CaF_2:5%Tm^{3+}-Y%Dy^{3+} for Y = 0 - 0.05 - 0.1 - 0.2 - 0.5 – 1 - 2. The Tm^{3+} doping ratio in the codoped system has been set to 5%; this choice is based on previous studies of Tm^{3+} doped CaF_2 crystals, as well as on Tm^{3+}-Dy^{3+} doped $LiYF_4$ and KY_3F_{10} crystals. It has been indeed proven that to enhance the cross-relaxation process between Tm^{3+} neighboring ions in fluorides, which is an essential phenomenon for the considered pumping scheme and the sensitization of Dy^{3+} ions through energy transfers, it is necessary to keep a high doping ratio in Tm^{3+} ions (>2%) in order to promote a clustering effect [21]. Moreover, it is also important to prevent a quenching of the Tm^{3+} $^3F_4$ level lifetime that could occur if the Tm^{3+} concentration is too high, hence this choice to set the Tm^{3+} doping ratio at 5 at. %.

The used precursors are CaF_2, Tm_2O_3 and Dy_2O_3 powder with a 4N purity. The rare earth oxide precursors are fluorinated by using NH_4HF_2 as fluorinating agent, following the chemical reaction:

$$Tm_2O_3 + 6\ NH_4HF_2 \rightarrow 2\ TmF_3 + 6\ NH_4F + 3\ H_2O\ ;\ T=180°C$$

The cake obtained at the end of this reaction is then annealed into a fluorination furnace at 650°C during few hours under argon atmosphere, in order to finish the fluorination reaction and to evacuate the residual water and –OH radicals, as well as the excess of NH_4F.

Once the crystal growth has been performed, the bulk crystals present a diameter of 6 mm and are cut into small cylinders of few millimeters thick; both faces of the crystals are finally polished so as to achieve a roughness in the order of hundred nanometers for spectroscopic experiments.

2.2 Spectroscopic experiments details

The absorption spectra were first recorded with a Perkin-Elmer Lambda1050 spectrophotometer, using a 0.75 nm spectral resolution throughout the 600 nm to 2500 nm spectral range, while a 370 NEXUS Nicolet FTIR spectrophotometer is used to complete the collection of the absorption spectra in the [2500-3600 nm] range.

The emission spectra were performed by exciting the samples with a Coherent 890 tunable Ti:Sapphire laser pumped by a Verdi V6 visible laser. The detection chain for collecting the emission spectra consists in a HRS2 Jobin-Yvon monochromator equipped with a 2 µm blazed grating with 300 grooves per millimeters, a nitrogen cooled InSb detector coupled to a Stanford Research Systems SR830 lock-in amplifier.

The fluorescence decays are measured by using a Continuum Horizon optical parametric oscillator pumped by a Continuum Surelite frequency tripled Nd:YAG pulsed laser to excite the samples; an Oriel monochromator associated with the same InSb detector are used for the detection.

3. Results and discussion

3.1 Spectroscopic study of Dy^{3+}-doped CaF_2 crystals

In view of the absorption spectra recorded in the [700-2000 nm] spectral range of Dy^{3+} ions in CaF_2 displayed in figure 1 and the corresponding energy diagram of figure 2, it is possible to assign these absorption bands centered at 751 nm, 800 nm, 905 nm, 1089 nm, 1275 nm and 1690 nm to the : $^6H_{15/2}\rightarrow{}^6F_{3/2}$, $^6H_{15/2}\rightarrow{}^6F_{5/2}$, $^6H_{15/2}\rightarrow{}^6F_{7/2}$, $^6H_{15/2}\rightarrow{}^6H_{7/2}+{}^6F_{9/2}$, $^6H_{15/2}\rightarrow{}^6H_{9/2}+{}^6F_{11/2}$ and $^6H_{15/2}\rightarrow{}^6H_{11/2}$ transitions respectively. The absorption bands centered at 800 and 905 nm present a particular interest for pumping schemes using commercially available laser diodes, the 905 nm absorption peak being stronger than the 800 nm one. Nevertheless, the necessity of a strong absorbed pump power requires high Dy^{3+} concentration which is not compatible with the three laser scheme imposed by the 3µm $^6H_{13/2}\rightarrow{}^6H_{15/2}$ transition (figure 2). When pumped at 800 nm or 905 nm, the Dy^{3+} ions in the $^6F_{5/2}$ and $^6F_{7/2}$ energy levels relax non-radiatively to the $^6H_{11/2}$ level. The $^6H_{11/2}\rightarrow{}^6H_{13/2}$ transition can be radiative around 4.3 µm but this emission is mainly quenched in fluoride hosts by multiphonon relaxation and thus less favorable than the $^6H_{13/2}\rightarrow{}^6H_{15/2}$ transition that occurs around 2.9 µm.

Following the absorption spectra presented in Figure 1, emission spectra of singly doped Dy^{3+}: CaF_2 crystals have been recorded around 2.9 µm, following an excitation at 900 nm and 804 nm. The normalized fluorescence spectra are reported in figure 3 and present broad emission bands, with a maximum peak at 2838 nm. These spectra show, that the CaF_2:0.2% Dy^{3+} and 2% Dy^{3+} crystals present a similar emission spectrum that peaks at 2838 nm when pumped at 804 nm or 900 nm. Moreover these spectra present a shoulder at 2920 nm, which is more pronounced in CaF_2:0.2% Dy^{3+} with an excitation at 900 nm than at 804 nm. It can be observed that this shoulder tends to disappear in CaF_2:2% Dy^{3+}. This shoulder is most likely related to the existence of different incorporation sites of Dy^{3+} ions in CaF_2.

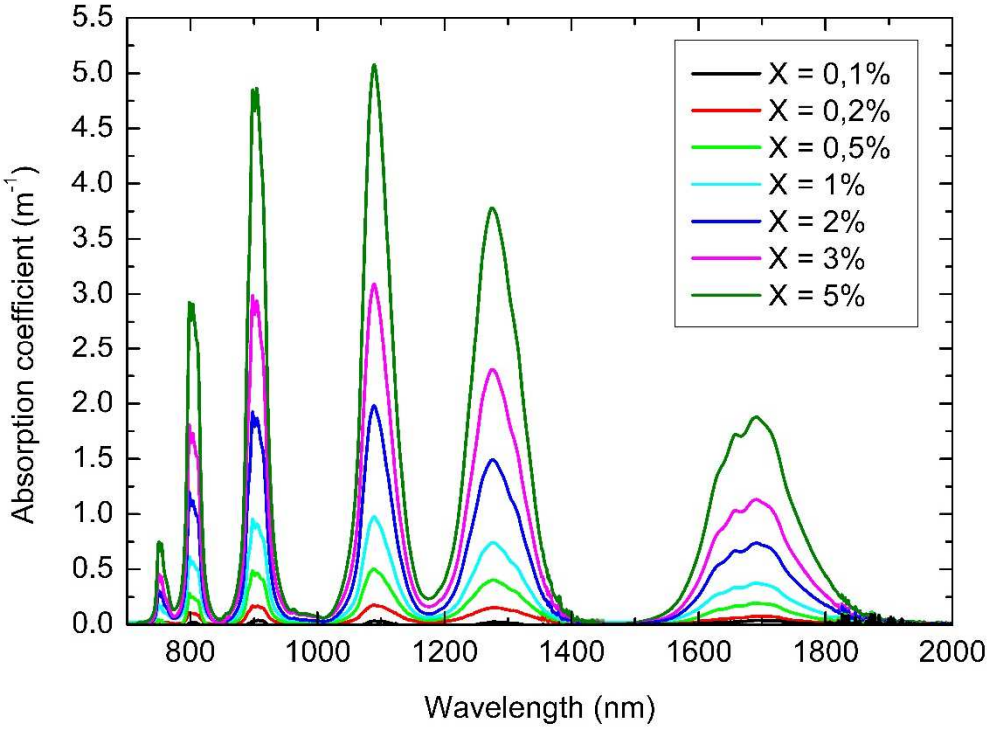

Figure 1: Absorption spectra in the [700 - 2000 nm] spectral range of CaF_2 crystals respectively doped with X % of Dy^{3+} ions

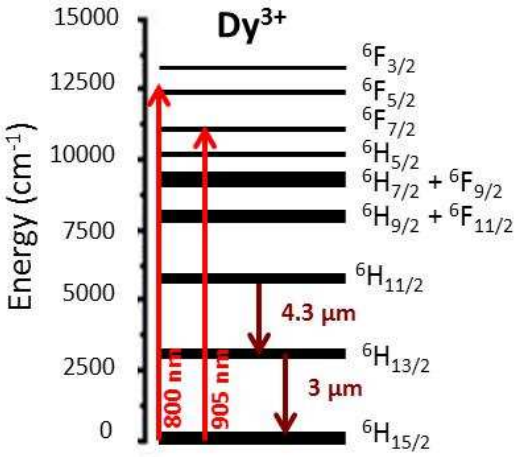

Figure 2: Energy levels and main radiative transitions in Dy^{3+} doped CaF_2 crystals

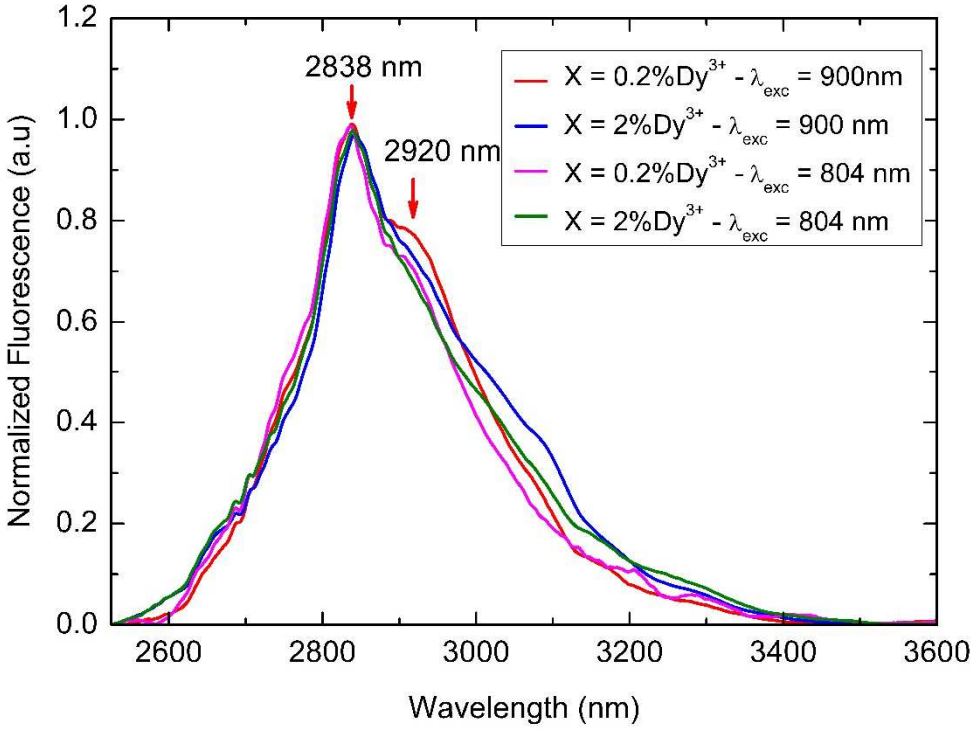

Figure 3: Fluorescence spectra of CaF_2:X % Dy^{3+} excited at 804 nm and 900 nm

In a complementary way, the fluorescence lifetimes of the $^6H_{13/2}$ level excited at 900 nm have been measured for various Dy^{3+} concentrations in CaF_2 and compared to other fluoride host matrices like ZBLAN glass [37], $LiYF_4$ and KY_3F_{10} crystals [21], as depicted in figure 4 and summarized in table 1. These fluorescence lifetimes strongly decrease with the Dy^{3+} concentration because of concentration quenching. Nevertheless it is worth noticing that at concentrations lower than 0.2% Dy^{3+}, the $^6H_{13/2}$ fluorescence lifetime is significantly longer in CaF_2 than in ZBLAN, whereas the $^6H_{13/2}$ lifetime is similar over 0.5% of Dy^{3+}.

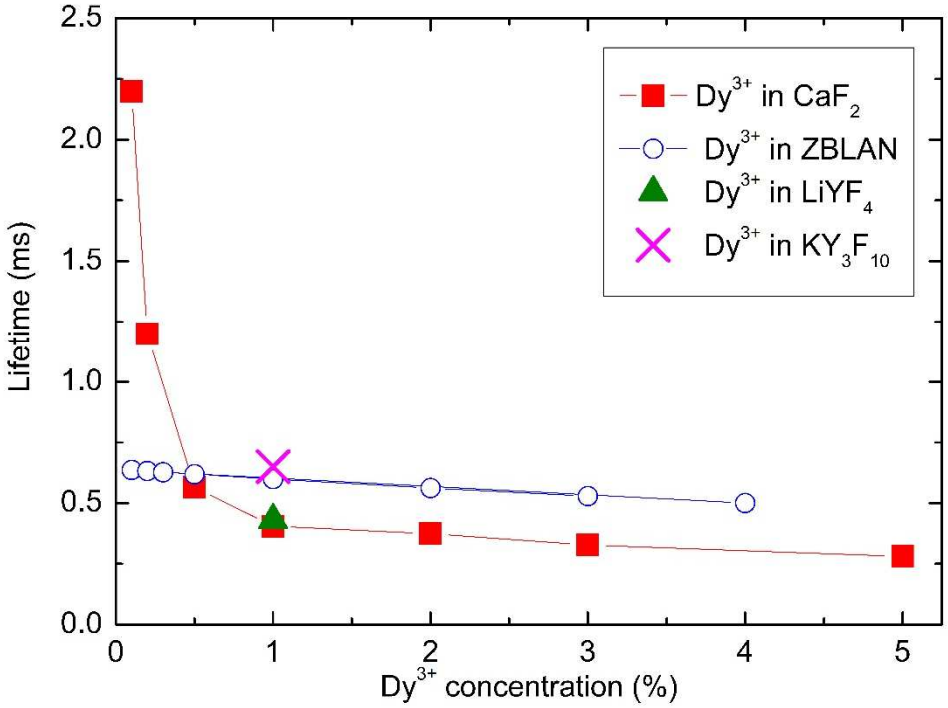

Figure 4: Lifetimes measurements of Dy^{3+} $^6H_{13/2}$ level in various host matrices

	τ_{fluo} of the $^6H_{13/2}$ level	τ_{rad} of the $^6H_{13/2}$ level
CaF_2: 5%Dy	280 µs	
CaF_2: 3%Dy	330 µs	
CaF_2: 2%Dy	375 µs	
CaF_2: 1%Dy	405 µs	47.5 ms
CaF_2: 0.5%Dy	565 µs	
CaF_2: 0.2%Dy	1.2 ms	
CaF_2: 0.1%Dy	2.2 ms	
ZBLAN: 0.5%Dy	631 µs [37]	46.8 ms [37]
$LiYF_4$: 1%Dy	430 µs [21]	38.6 ms
KY_3F_{10}: 1%Dy	650 µs [21]	36.1 ms

Table 1: Summary of the $^6H_{13/2}$ measured lifetimes (τ_{fluo}) and radiative lifetimes (τ_{rad}) when excited at 900 nm

The $^6H_{13/2}$ radiative lifetime in CaF_2 has been calculated using the Judd-Ofelt analysis [38] and found to be 47.5 ms, which is similar to other host matrices like ZBLAN, $LiYF_4$ or KY_3F_{10}, (table 1). In all host matrices, a strong difference between τ_{rad} and τ_{fluo} can be observed because of multiphonon relaxations and also to concentration quenching when increasing the dopant concentration. This issue is a key factor to be addressed in order to achieve decent laser performance.

In order to limit the shortening of the $^6H_{13/2}$ fluorescence lifetimes at 2.9 µm the Dy^{3+}concentrations must be kept at 0.5%, or below. To ensure a strong absorption of the pump beam despite a low Dy^{3+}concentration, we investigated codoped systems, where the pump energy is absorbed by sensitizer ions such as Tm^{3+} ions and transfered towards the Dy^{3+} emitting ions. This codoping has the further advantage to preserve a small quantum defect while pumping at 800 nm. .

3.2 Spectroscopic study of codoped Tm^{3+}-Dy^{3+} : CaF_2 crystals

The codoped Tm^{3+}-Dy^{3+}: CaF_2 crystals present a strong absorption band centered around 767 nm, as shown in figure 5, due to the Tm^{3+} $^3H_4$ level absorption ($^3H_6 \rightarrow {}^3H_4$), which can be easily pumped with commercially available laser diodes. At high enough dopant concentration, the Tm^{3+} excitation can be efficiently transferred to the Dy^{3+} ions via energy transfer processes that take place in two steps. These energy transfers are made even more efficient by the rare earth clustering effect, which takes place in CaF_2. Once the Tm^{3+} ions have been excited in the $^3H_4$ level, a very efficient cross relaxation process occurs between two neighboring Tm^{3+} ions within Tm^{3+} clusters and brings them both into the metastable $^3F_4$ energy level, as described in the energy diagram given in figure 6. This known cross-relaxation process is remarkable because it leads to the excitation of two Tm^{3+} ions after the excitation of only one Tm^{3+} ion. The second step of this process is the energy transfer from Tm^{3+} ions to Dy^{3+} ions, which is made efficient thanks to a strong spectral overlap between the Tm^{3+} emission band ($^3F_4 \rightarrow {}^3H_6$) and the Dy^{3+} absorption band ($^6H_{15/2} \rightarrow {}^6H_{11/2}$), as shown in figure 5(b). Once excited in the $^6H_{11/2}$ level Dy^{3+} ions quickly relax non radiatively down to the $^6H_{13/2}$ emitting level, which subsequently relax radiatively down to the $^6H_{15/2}$ ground state level emitting thus a fluorescence around 2.9 µm. So, this two-steps Dy^{3+} excitation scheme allows a significant increase of the quantum efficiency of Tm^{3+}-Dy^{3+} codoped systems for an emission around 2.9 µm.

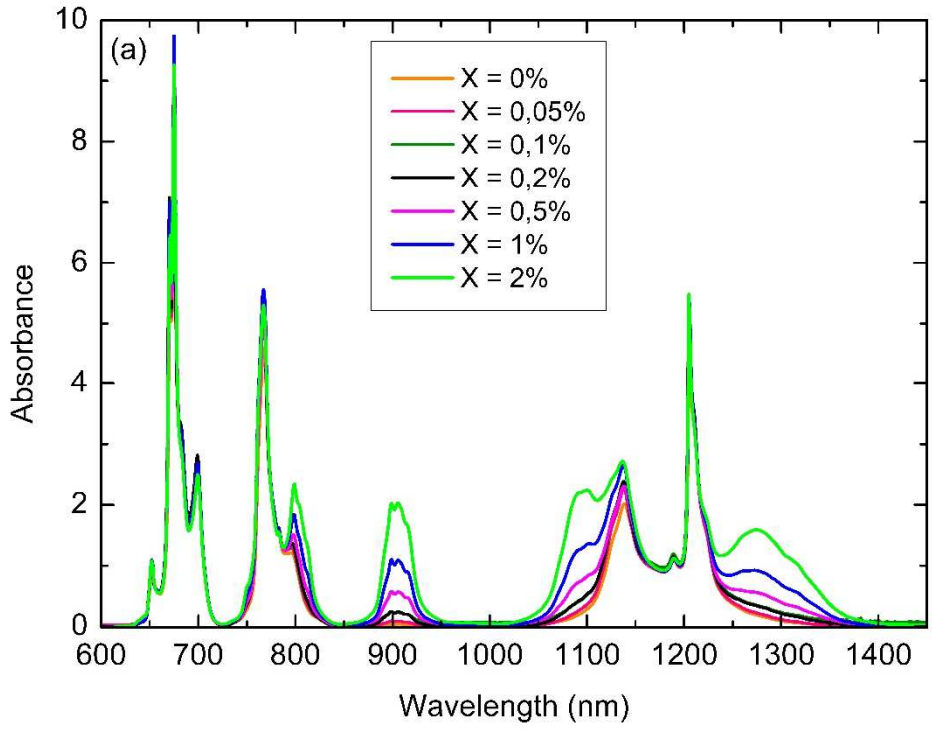

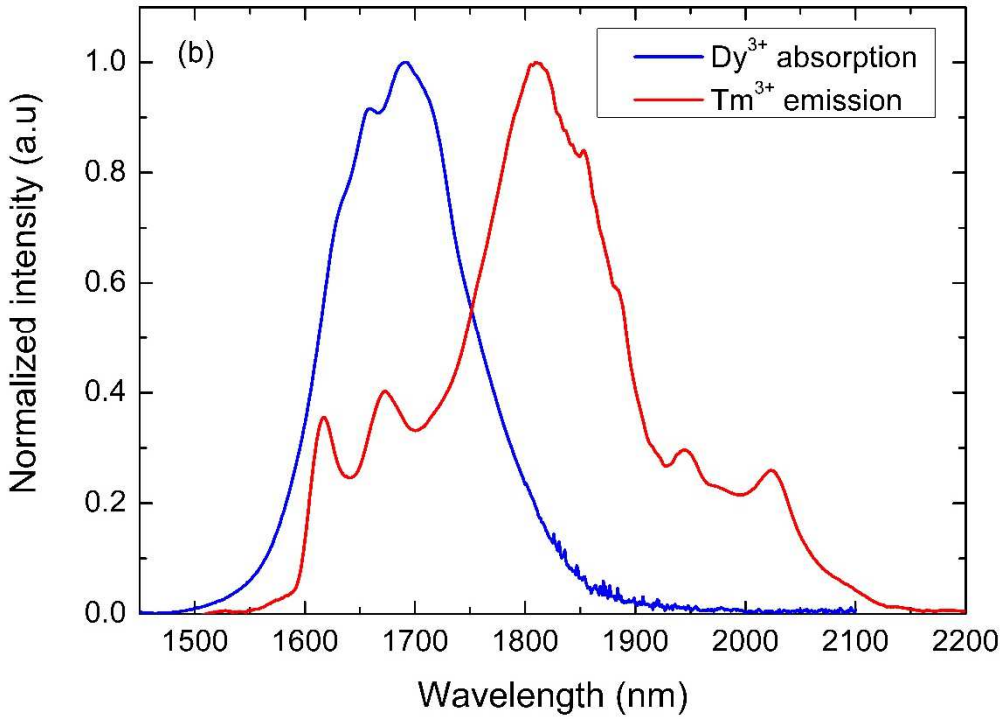

Figure 5: (a) Absorption spectra of the codoped 5% Tm^{3+}- X% Dy^{3+}:CaF_2 crystals in the [600 -1450 nm] spectral range, (b) Spectral overlap between the emission band of Tm^{3+} ions and the absorption band of Dy^{3+} ions in CaF_2 in the [1450-2200 nm] spectral range

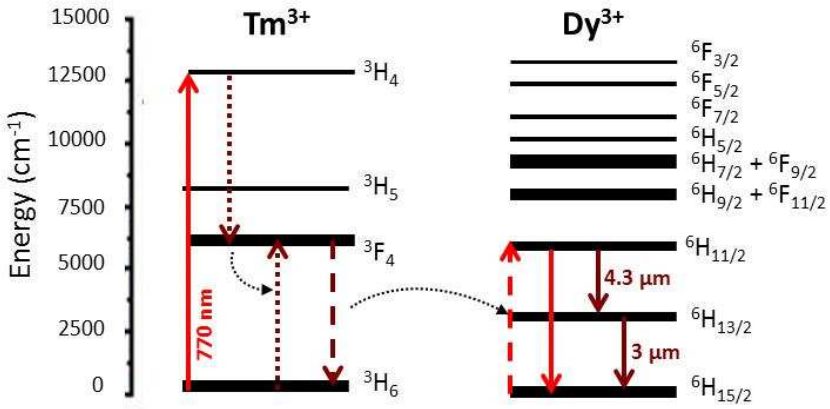

Figure 6: Energy levels, main radiative transitions and energy transfer processes in Tm^{3+}-Dy^{3+} doped CaF_2 crystals

The energy transfer efficiency from Tm^{3+} to Dy^{3+} ions ($^3F_4$, $^6H_{15/2} \rightarrow {}^3H_6$, $^6H_{11/2}$) can be highlighted by measuring the Tm^{3+} $^3F_4$ level lifetime at 1.9 µm ($^3F_4 \rightarrow {}^3H_6$ transition), in Tm^{3+} singly doped and Tm^{3+}-Dy^{3+} codoped CaF_2 crystals. Table 2 summarizes the Tm^{3+} $^3F_4$ level and Dy^{3+} $^6H_{13/2}$ level fluorescence lifetimes in various Tm^{3+}-Dy^{3+} codoped CaF_2 samples.

One can observe in Table 2 that the $^3F_4$ lifetime in 5%Tm doped CaF_2 is 17 ms and strongly decreases to 60 µs in CaF_2:5%Tm^{3+}-2%Dy^{3+}. This strong decrease in lifetime evidences the efficiency of the Tm^{3+} to Dy^{3+} energy transfer, which is further confirmed by the fluorescence spectra shown in figure 7. Indeed, the intensity of the Tm^{3+} emission band centered around 1.85 µm ($^3F_4 \rightarrow {}^3H_6$ transition) after a 767 nm excitation, is strongly reduced when codoping with 0.5% Dy^{3+} and completely quenched at higher Dy^{3+} concentration.

	$\tau_{fluo}(\lambda_{exc}$=900 nm, Dy^{3+} $^6H_{13/2}$ level)	$\tau_{fluo}(\lambda_{exc}$=767 nm, Tm^{3+} $^3F_4$ level)
CaF_2 : 5%Tm^{3+}-2%Dy^{3+}	475 µs	60 µs
CaF_2 : 5%Tm^{3+}-1%Dy^{3+}	505 µs	120 µs
CaF_2 : 5%Tm^{3+}-0.5%Dy^{3+}	590 µs	270 µs
CaF_2 : 5%Tm^{3+}-0.2%Dy^{3+}	640 µs	630 µs
CaF_2 : 5%Tm^{3+}-0.1%Dy^{3+}	620 µs	890 µs
CaF_2 : 5%Tm^{3+}-0.05%Dy^{3+}	630 µs	1.85 ms
CaF_2 : 5%Tm^{3+}	-	17 ms

Table 2: Summary of the measured lifetimes (τ_{fluo}) of the Dy^{3+} $^6H_{13/2}$ level when excited at 900 nm and of the Tm^{3+} $^3F_4$ level when excited at 767 nm

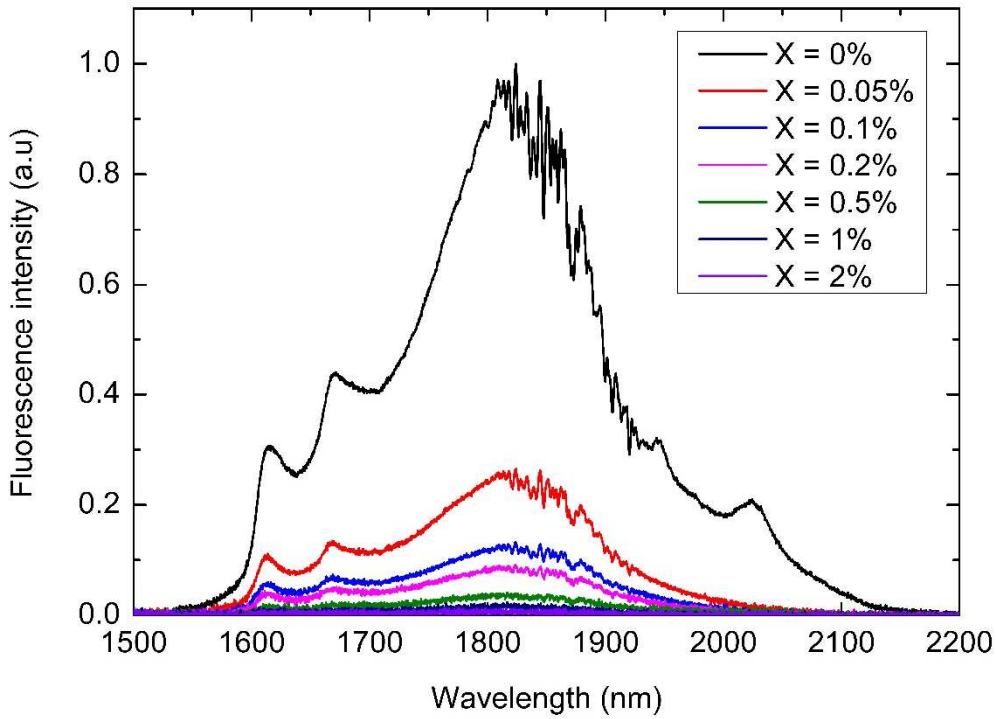

Figure 7: Fluorescence spectra around 1.9 µm of the CaF_2:5%Tm and CaF_2:5%Tm-X%Dy crystals excited at 767 nm

To further evidence the impact of the Tm codoping, we have recorded the Dy^{3+} emission intensity around 2.9 µm in two different CaF_2 crystals with the same Dy^{3+} doping level and the same excitation density: namely a 5%Tm^{3+}-0.2% Dy^{3+} codoped CaF_2 excited at 767 nm and a 0.2% Dy^{3+} doped CaF_2 excited at 900 nm, as presented in figure 8. The advantage of Tm codoping is here clearly demonstrated: the Dy^{3+} fluorescence intensity around 2.9 µm is more than 6 times higher in the Tm^{3+}-Dy^{3+} codoped sample excited through the Tm^{3+} sensitizers, compared to the singly doped Dy^{3+}:CaF_2 crystal which is directly excited at 900 nm.

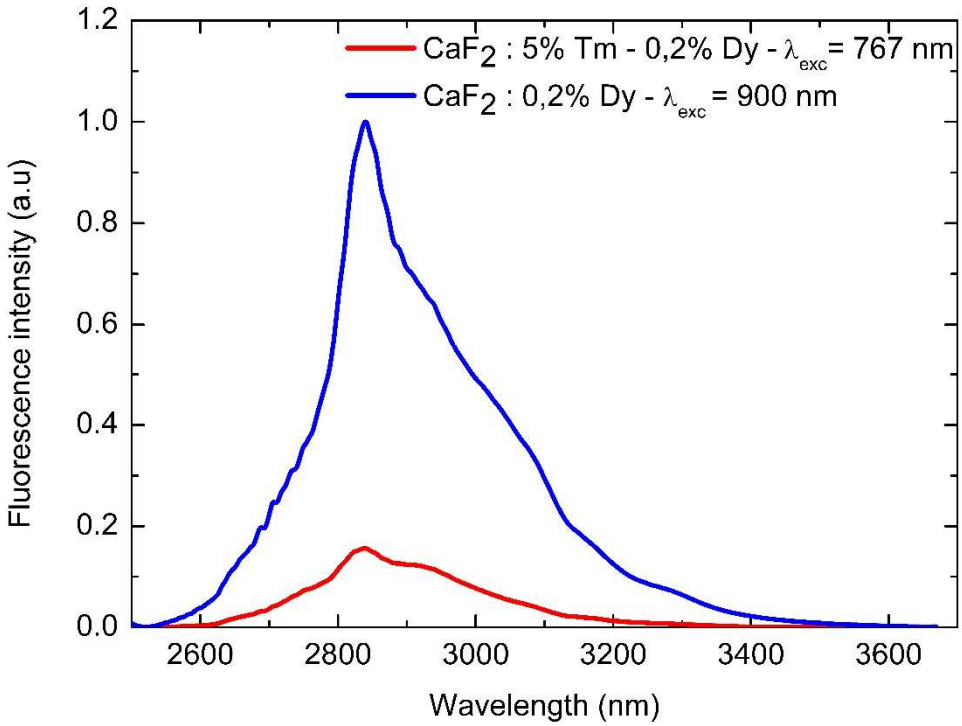

Figure 8: Fluorescence spectra around 3µm of 5%Tm^{3+}-0.2%Dy^{3+} and 0.2%Dy^{3+} doped CaF_2 crystals respectively excited at 767 nm and 900 nm with the same excitation density.

Using the Tm^{3+} $^3F_4$ fluorescence and radiative lifetimes (Table 2) it is possible to derive the energy transfer efficiency from Tm^{3+} to Dy^{3+} ions. This energy transfer efficiency η_{ET} is defined by the following expression:

$$\eta_{ET} = (1 - \frac{\tau}{\tau_0}) \quad (1)$$

where τ corresponds to the Tm^{3+} $^3F_4$ measured fluorescence lifetime at 1.85 µm ($^3F_4 \rightarrow {}^3H_6$ transition) in the 5%Tm^{3+}-X%Dy^{3+} codoped samples and τ_0 corresponds to the $^3F_4$ lifetime in a singly doped 5%Tm^{3+} crystal (τ_0 =17 ms) meaning without any energy transfer towards Dy^{3+} ions. Figure 9(a) depicts this energy transfer efficiency as a function of the Dy^{3+} concentration along with the Dy^{3+} $^6H_{13/2}$ level fluorescence lifetime. Figure 9(a) shows clearly the efficiency of the energy transfer that already occurs at very low Dy^{3+} concentration (0.05%). For concentrations higher than 0.5%, the energy transfer efficiency is close to unity, which means that almost all the energy absorbed by the Tm^{3+} sensitizers is transferred to Dy^{3+} ions, thanks to the presence of Tm-Dy clusters. In the meantime, the Dy^{3+} $^6H_{13/2}$

fluorescence lifetime drops significantly when increasing the Dy^{3+} concentration due to concentration quenching effects that occur between Dy^{3+} neighboring ions. As a conclusion of Figure 9(a), the Dy^{3+} concentration should be kept at 0.5% or below since the sensitization by Tm^{3+} ions is already very efficient at these low Dy^{3+} concentrations.

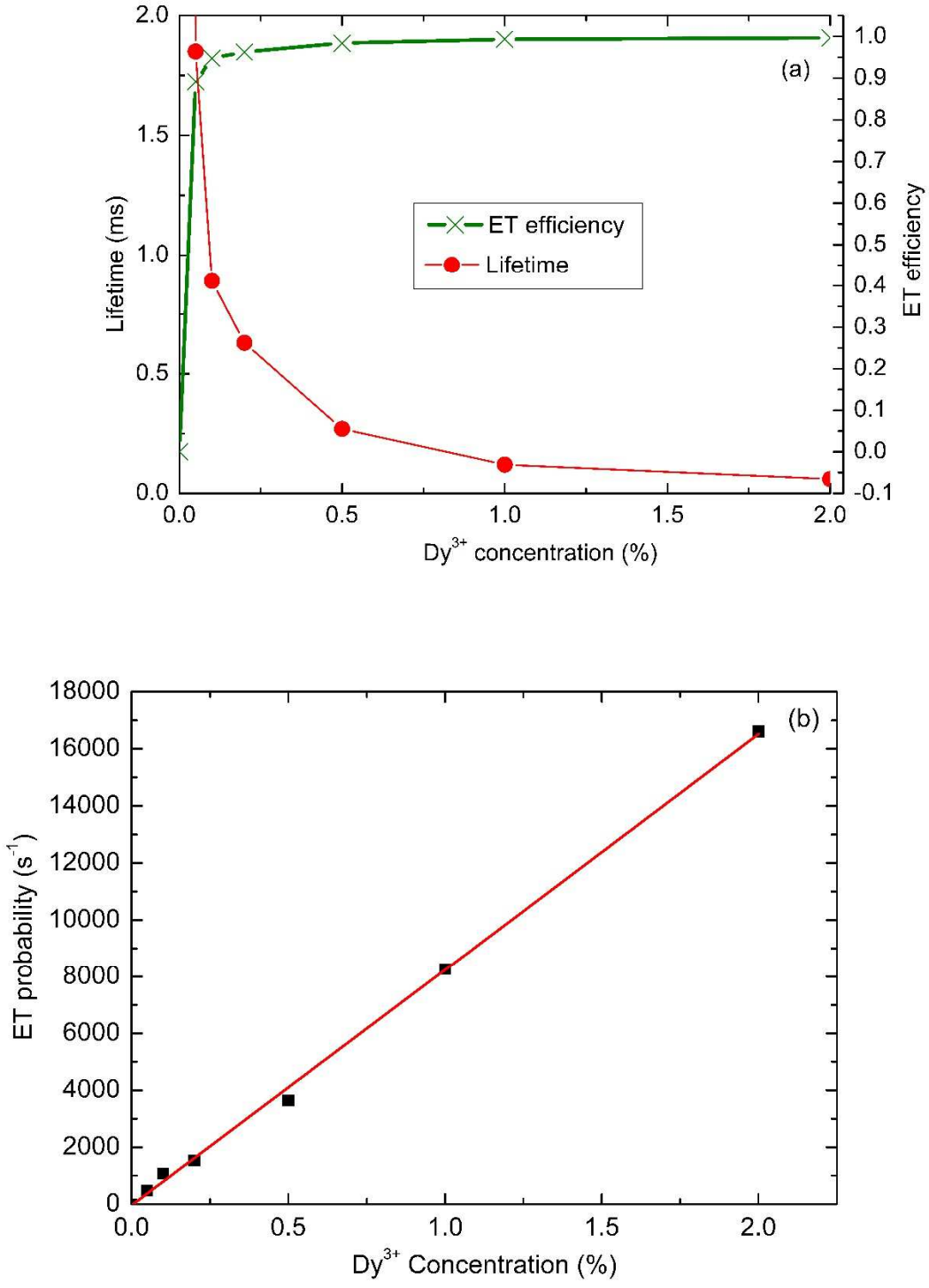

Figure 9: (a) Evolution of the Dy^{3+} $^6H_{13/2}$ fluorescence lifetime of 5%Tm - X% Dy codoped CaF_2 crystals versus the Tm to Dy energy transfer efficiency, as a function of the Dy^{3+} concentration (where

X = 0; 0.05; 0.1; 0.2; 0.5; 1; 2), (b) Tm^{3+} to Dy^{3+} energy transfer probability (A_{ET}) as a function of the Dy^{3+} concentration

In a complementary way, the energy transfer probability A_{ET} (s^{-1}) has been calculated as a function of the Dy^{3+} concentration N_{Dy} and is displayed in figure 9(b), according to the expression: $A_{ET} = \tau^{-1} - \tau_0$. It shows that the energy transfer probability is proportional to the Dy^{3+} acceptor concentration, which is typical of energy transfer mechanisms among rare-earth ions between donors (here Tm^{3+} ions) and acceptors (Dy^{3+} ions). Moreover, it becomes possible to determine the energy transfer parameter $W_{Tm\text{-}Dy}$ ($cm^3.s^{-1}$) from Tm^{3+} to Dy^{3+} ions, by calculating the slope of this linear dependence $A_{ET}=f(N_{Dy})$ in figure 9(b). The $W_{Tm\text{-}Dy}$ parameter is found equal to 3.38 $x10^{-17}$ $cm^3.s^{-1}$ and represents a key parameter for the modeling of laser operation around 3 µm in Tm^{3+}-Dy^{3+} codoped systems which will be discussed in the next section.

3.3 Laser potential of Dy^{3+}-doped and Tm^{3+}-Dy^{3+} codoped CaF_2 crystals around 3 µm

3.3.1 Laser gain cross section of Dy^{3+}:CaF_2

The laser gain cross-section $\sigma_g(\lambda)$ of Dy^{3+} in CaF_2 is calculated, according to the following relationship Eq 2.a [39]:

$$\sigma_g(\lambda) = \beta.\sigma_{em}(\lambda) - (1-\beta).\sigma_{abs}(\lambda) \text{ (Eq 2.a)},$$

where β is the population inversion coefficient such as $\beta = N_2/N_1$, where N_2 and N_1 are the populations of the $^6H_{13/2}$ and $^6H_{15/2}$ levels respectively; $\sigma_{abs}(\lambda)$ and $\sigma_{em}(\lambda)$ are respectively the absorption cross-section and the emission cross-section of the Dy^{3+} $^6H_{13/2} \rightarrow {}^6H_{15/2}$ transition around 3µm.

The emission cross-section $\sigma_{em}(\lambda)$ is calculated thanks to the well-known Füchtbauer-Ladenburg relationship given by Eq 2.b and by using the results of the spectroscopic study presented in the previous section:

$$\sigma_{em}(\lambda) = \frac{B}{8.\pi.n^2.c.\tau_R} \frac{\lambda^5.I(\lambda)}{\int_{\lambda 1}^{\lambda 2} I(\lambda).d\lambda} \text{ (Eq. 2.b)},$$

where, B is the branching ratio, c is the light speed, τ_R is the radiative lifetime of the emitting level, $I(\lambda)$ is the emission intensity as a function of the wavelength.

By this way, we determined the Dy^{3+} emission cross-section in CaF_2 at 3.1 µm σ_{em}(3100 nm), so that $\sigma_{em}(3100\text{ nm}) = 0.165 \times 10^{-20}$ cm^2, while its absorption cross-section at the same wavelength is $\sigma_{abs}(3100\text{ nm}) = 0.0331 \times 10^{-20}$ cm^2. Thus, it becomes possible to calculate the gain cross sections for various inversion population coefficients β, as presented in figure 10.

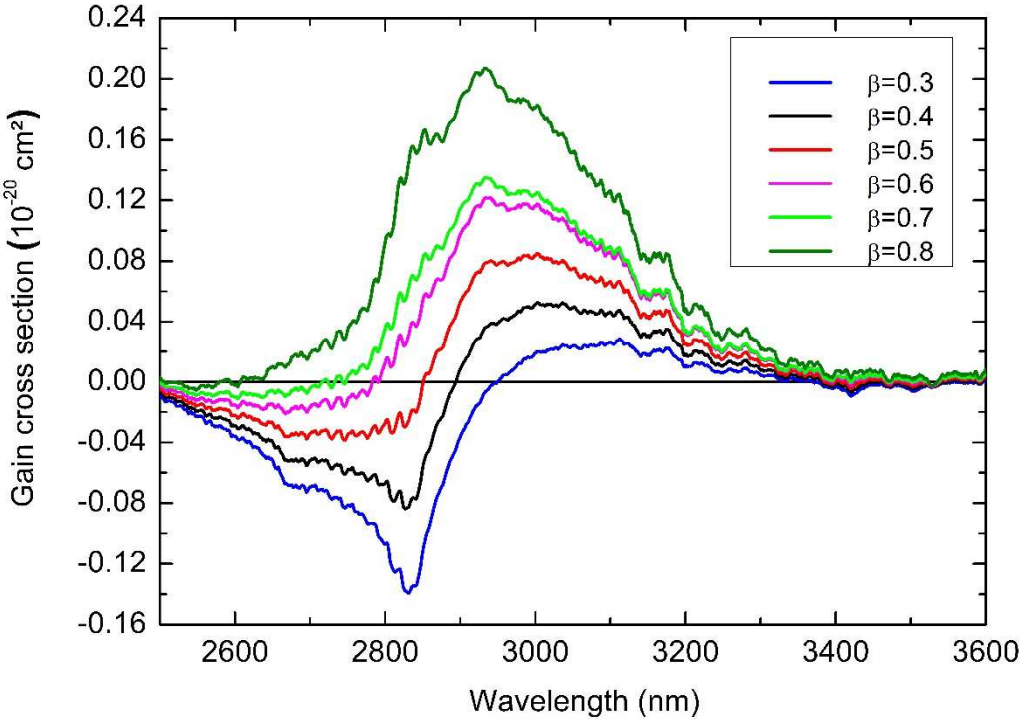

Figure 10: Calculated gain cross section of Dy^{3+} in CaF_2 for different values of population inversion

Figure 10 shows that a 30% population inversion (β=0.3) is required to reach a positive laser gain around 3 µm and thus to be able to achieve Dy^{3+} laser emission. For this purpose, promising laser perspectives can be expected in a waveguide configuration. The poor emission quantum efficiency of the $^6H_{13/2}$ emitting level highlighted by the lifetimes measurements in Table 1, will necessarily bring about a high laser threshold which can be difficult to attain in a standard bulk laser crystal configuration. This laser threshold can however be reached more easily in a waveguide configuration, as it has been previously demonstrated for Dy^{3+} doped ZBLAN optical fibers with low Dy^{3+} concentration (~ 0.1% at.) [15]. Indeed, high laser efficiencies around 2.9 µm have been reached in such optical fibers thanks to low Dy^{3+} concentrations, combined with the length of the gain medium and the confinement of the laser modes in the guiding medium [15]. In the case of crystalline waveguides, it is not possible to achieve the length of an optical fiber, which can be meters long, allowing thus very low dopant concentrations. Nevertheless, this limitation can be balanced by a quite higher Dy^{3+} concentration in CaF_2 waveguides, which are centimeter long and present stronger absorption and emission cross-sections than a glassy medium like ZBLAN.

3.3.2 Modeling of the laser efficiency around 3 µm of Dy^{3+} doped CaF_2 waveguides

To perform the modeling of the laser efficiency around 3 µm of Dy^{3+}-doped CaF_2 waveguides, a 1 cm long linear waveguide with a section of 35 × 35 µm² and a refractive index contrast of 1×10^{-3} between the doped guiding layer and its undoped substrate, have been considered. These waveguide dimensions would be small enough to present a transverse single mode behavior at 3.1µm, as well as

thick enough to minimize the scattering optical losses and the coupling losses of the pump. We then envisioned two different pump wavelengths (λ_p) at 900 nm and 1690 nm, which could be emitted by a Ti:Saphire laser and a Raman shifted Er-doped laser fiber respectively. Both types of pump sources typically exceed the Watt level in output power. These two pump wavelengths offer different advantages. The pumping at 1690 nm strongly reduces the quantum defect, while the pump energy is better absorbed by the Dy^{3+}-doped CaF_2 waveguides at 900 nm because of a higher absorption cross-section.

Previous works have demonstrated that it is possible to get very high optical quality waveguides along a 1 cm length l, like in Tm^{3+}-doped $LiYF_4$ crystalline planar waveguides elaborated by Liquid Phase Epitaxy (LPE), for which optical losses as low as 0.11 dB/cm, corresponding to ~2.5% of optical losses, have been achieved [40]. The modeling presented here, considers optical losses as high as 6.5 % (~0.3 dB/cm) along a round trip in a 1 cm long waveguide. Indeed, it is a typical optical losses level, which is frequently observed in such crystalline waveguides.

Two different approaches have been considered and compared: a classic 3-levels scheme analytic model labeled as theoretical and a numerical modeling labeled as model.

The analytic model leads to the calculation of the theoretical laser threshold $P_{thr}^{theoretical}$ and the theoretical slope efficiency $\eta^{theoretical}$, according to equations (Eq. 3) and (Eq. 4) [41]:

$$P_{thr}^{theoretical} = \frac{h\nu_P \pi\, \omega_p^2}{n_{abs}(\sigma_{abs}(\lambda)+\sigma_{em}(\lambda))\tau}\left(\sigma_{abs}(\lambda)\, N_{Dy} l + \frac{-\mathrm{Ln}(1-T_{OC})-\mathrm{Ln}(1-L)}{2}\right) \text{ (Eq. 3)},$$

$$\eta^{theoretical} = \frac{h\nu_L}{h\nu_P} n_{abs} \frac{\mathrm{Ln}(1-T_{OC})}{\mathrm{Ln}(1-T_{OC})+\mathrm{Ln}(1-L)} \text{ (Eq. 4)},$$

where h is the Planck constant, ν_p is the frequency at the pump wavelength, ω_p is the radius of the pump laser beam waist, τ is the fluorescence lifetime of the Dy^{3+} $^6H_{13/2}$ emitting level, l is the waveguide length, T_{oc} is the output coupler transmission and L corresponds to the round-trip optical losses. n_{abs} refers to the pump absorption, which can be estimated by the following expression (Eq.5), considering that there is no saturation of the absorption:

$$n_{abs} \sim 1 - e^{-\sigma_{abs}(\lambda).N_{Dy}.l} \text{ (Eq. 5)}.$$

The numerical approach is based on the rate equations Eq.6a and Eq.6b, by considering a quasi-four level laser scheme:

$$\frac{dN_1}{dt} = -\sigma_{abs}^P N_1 I_p + \frac{N_2}{\tau_2} + \left(\sigma_{em}^L N_2 - \sigma_{abs}^L N_1\right) I_L \text{ (Eq.6a)},$$

$$\frac{dN_2}{dt} = \sigma_{abs}^P N_1 I_p - \frac{N_2}{\tau_2} - \left(\sigma_{em}^L N_2 - \sigma_{abs}^L N_1\right) I_L \quad \text{(Eq.6b)},$$

where N_1 and N_2 are the populations of the Dy^{3+} $^6H_{15/2}$ and $^6H_{13/2}$ levels respectively, while I_L and I_P represent the laser and pump beams intensity respectively, which are expressed in photons/cm². σ^P_{abs} is the absorption cross-section at the pump wavelength λ_P; σ^L_{abs} and σ^L_{em} are the absorption and emission cross-sections at the laser wavelength λ_L; τ_2 is the emitting laser level lifetime.

The numerical model requires first the discretization of the pump intensity along the propagating z axis, according to Eq.6c, as well as the calculation of the average signal gain S_g along the same direction in the gain medium according to Eq.6d:

$$I_p(z+dz) = I_p(z) - \left(\sigma_{abs}^{P} N_1 dz\right).I_p(z) \qquad \text{(Eq.6c)},$$

$$S_g = \sum\left(\sigma_{em}^{L} N_2 - \sigma_{abs}^{L} N_1\right) dz \quad \text{(Eq.6d)},$$

The intracavity laser intensity I_L is then calculated considering Eq.6e:

$$\frac{dI_L}{dt} = \left(S_g + \frac{\mathrm{Ln}(R(1-L))}{2}\right)\frac{c}{l_{cav}} I_L \quad \text{(Eq.6e)},$$

where R is the output coupler reflectivity, c is the speed of light and l_{cav} is the cavity length.

In this manner, the numerical model leads to the output power P_{out}^{model} at the laser wavelength according to Eq.6f:

$$P_{out}^{model} = I_L \frac{1-R}{1+R} h v_l \pi {\omega_l}^2 \qquad \text{(Eq.6f)},$$

where ω_l is the laser mode radius. In addition, it is assumed that the overlap between the pump and laser modes is equal to unity and that the spatial profiles of both pump and laser beams are top-hat beams.

By this way, it becomes possible to determine the laser threshold P_{thr}^{model} (W), as well as the laser slope efficiency η^{model}.

The laser performance of Dy^{3+}-doped CaF_2 waveguides have been compared by pumping at 900 nm and at 1690 nm, for various Dy^{3+} concentrations (N_{Dy}) which have been investigated in this work, i.e. 1%, 2%, 3% and 5% Dy^{3+}. At 1690 nm, the absorption cross-section σ_{abs}(1690 nm) is equal to 1.44 $\times 10^{-21}$ cm², while at 900 nm, σ_{abs}(900 nm) = 3.8 $\times 10^{-21}$ cm². In such conditions, the simulations show that a 15% transmission output coupler is required to open sufficiently the laser cavity, while keeping a reasonable laser threshold at the same time. Considering the hypothesis mentioned above, the laser modeling results for both pump wavelengths are presented in figure 11 and summarized in table 3.

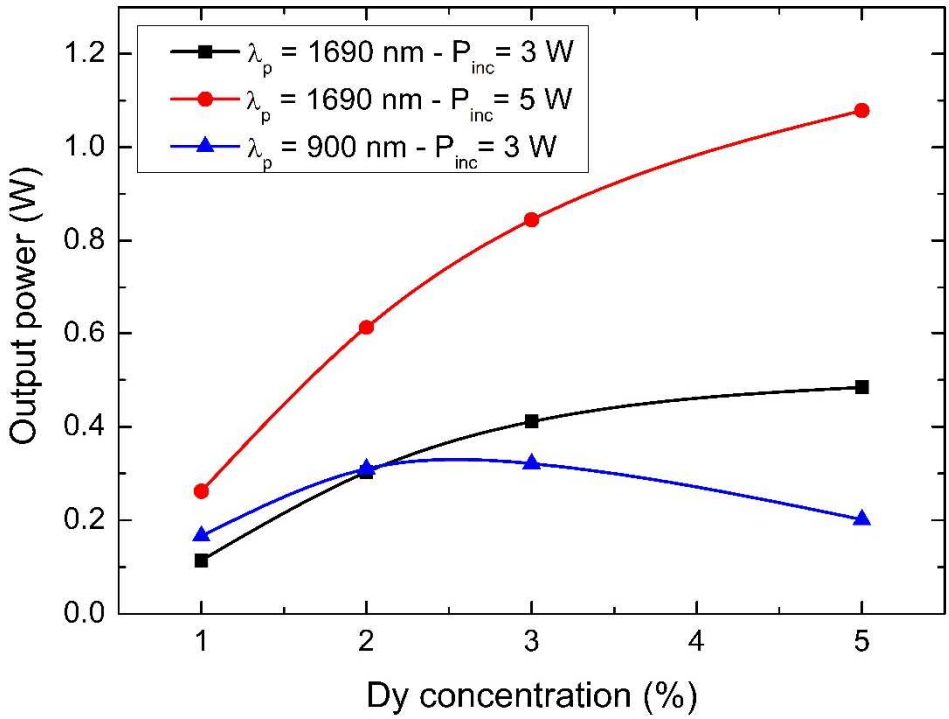

Figure 11: Laser output power at 3.1 µm of Dy^{3+} doped CaF_2 waveguide for a 15% transmission output coupler as a function of the Dy^{3+} concentration, for different pump wavelength and incident pump power

λ_p (nm)	1690	1690	1690	1690	900	900	900	900
N_{Dy}(%)	1	2	3	5	1	2	3	5
n_{abs}(%)	19.3	40.6	56.7	77.7	44.3	76.9	91.2	99.1
P_{thr}^{model} (W)	1.50	1.10	1.15	1.40	1.17	1.05	1.27	2.00
$P_{thr}^{theoretical}$ (W)	1.43	1.04	1.10	1.36	1.17	1.03	1.28	2.01
η^{model} (%)	7.4	15.5	21.7	29.7	9.1	15.8	18.6	20.3
$\eta^{theoretical}$ (%)	7.4	15.6	21.9	30.0	9.1	15.8	18.7	20.4

Table 3: Summary of the modeled and theoretical laser results for various Dy^{3+} doping levels and pump wavelengths

The theoretical laser thresholds $P_{thr}^{theoretical}$ lie between 1W and 2W for both pump wavelengths, as summarized in table 3, which are reasonable pump powers to consider the development of such 35 × 35 µm² Dy^{3+}-doped CaF_2 ridge waveguides for laser applications around 3.1 µm. The maximum slope efficiency, which can be reached in such cases, is evaluated to 30% as a function of the incident pump power. It corresponds to an output power in the order of the Watt level for a pumping at 1690 nm and in the order of few hundreds of mW for a pumping at 900 nm when considering the analytic expression of $\eta^{theoretical}$ (Eq. 4).

As indicated in table 3, the results that have been numerically calculated for this study, are consistent with the classic 3-levels scheme analytic model. Moreover, the numerical model can be considered as more accurate since it allows the calculation of the real absorbed pump power at the laser threshold, by taking into account the saturation of the absorption within the waveguide.

Concerning the pumping at 900 nm, a 5% Dy^{3+} doping level does not appear to be interesting, as illustrated by figure 11: the laser threshold in this case is calculated to be around 2 W, whereas it lies around 1 W for lower doping concentrations. As shown in Figure 11, a 2% Dy^{3+}-doped CaF_2 waveguide should allow the extraction of around 300 mW of output power at 3.1 µm, if a pump power of at least 3 W is available at 900 nm. The 1 cm long waveguide would absorb 77% of the incident pump power in a 2% Dy^{3+}-doped CaF_2, whereas a 5% Dy^{3+}-doped CaF_2 waveguide would absorb 99%, as summarized in table 3. Considering the quasi-3 levels nature of this laser transition, this very strong absorption is detrimental and the waveguide length should be shortened for a 5% Dy^{3+}-doped CaF_2 waveguide.

In the case of a pumping at 1.69 µm, the laser threshold lies between 1W and 1.5 W for the considered Dy^{3+} doping ratios (table 3). Thus, the most promising laser performance, which exceeds the watt in output power, is reached by considering a 5 W incident pump power, as well as a 5% Dy^{3+} doping level for a 1 cm long ridge waveguide.

3.3.3 Modeling of the laser efficiency around 3 µm of Tm^{3+}-Dy^{3+} doped CaF_2 waveguides

The performances of the CW Tm^{3+}-Dy^{3+} doped CaF_2 linear waveguides laser was modeled using the following rate-equation model (Eq.7a-f), accounting for the different steps of the involved excitation mechanism: (i) ground-state depletion for both Tm^{3+} and Dy^{3+} ions, (ii) Tm^{3+}-Tm^{3+} Cross-relaxation (CR) among neighboring Tm^{3+} ions and (iii) $Tm^{3+}(^3F_4) \rightarrow Dy^{3+}(^6H_{13/2})$ energy transfer (ET), before the Dy^{3+} radiative deexcitation ($^6H_{13/2} \rightarrow {}^6H_{15/2}$).

$$\text{Dy}(^6H_{15/2}): \frac{dN_1}{dt} = \frac{N_2}{\tau_2} - K_{TmDy}N_4N_1 + K_{DyTm}N_3N_2 + (\sigma_e N_2 - \sigma_{abs}N_1)I_L \qquad \text{(Eq.7a)}$$

$$\text{Dy}(^6H_{13/2}): \frac{dN_2}{dt} = -\frac{N_2}{\tau_2} + K_{TmDy}N_4N_1 - K_{DyTm}N_3N_2 - (\sigma_e N_2 - \sigma_{abs}N_1)I_L \qquad \text{(Eq.7b)}$$

$$\text{Tm}(^3H_6): \frac{dN_3}{dt} = K_{TmDy}N_4N_1 - K_{DyTm}N_3N_2 + \frac{N_4}{\tau_4} + \beta_{63}\frac{N_6}{\tau_6} - C_{CR}N_3N_6 - \sigma_{abs}^P N_3 I_p \qquad \text{(Eq.7c)}$$

$$\text{Tm}(^3F_4): \frac{dN_4}{dt} = -K_{TmDy}N_4N_1 + K_{DyTm}N_3N_2 - \frac{N_4}{\tau_4} + \frac{N_5}{\tau_5} + 2C_{CR}N_3N_6 + \beta_{64}\frac{N_6}{\tau_6} \qquad \text{(Eq.7d)}$$

$$\text{Tm}(^3H_5): \frac{dN_5}{dt} = -\frac{N_5}{\tau_5} + \beta_{65}\frac{N_6}{\tau_6} \qquad \text{(Eq.7e)}$$

$$\text{Tm}(^3H_4): \frac{dN_6}{dt} = \sigma_{abs}^P N_3 I_p - \frac{N_6}{\tau_6} - C_{CR}N_3N_6 \qquad \text{(Eq.7f)}$$

where N_1 and N_2 are the population rate of the $^6H_{15/2}$ (Dy^{3+}) and $^6H_{13/2}$ (Dy^{3+}) levels, while N_3, N_4, N_5 and N_6 are respectively the population rate of the $^3H_6$ (Tm^{3+}), $^3F_4$ (Tm^{3+}), $^3H_5$ (Tm^{3+}) and $^3H_4$ (Tm^{3+}) levels. τ_1, τ_2, τ_3, τ_4, τ_5, τ_6 are respectively the lifetimes of the levels $^6H_{15/2}$ (Dy^{3+}), $^6H_{13/2}$ (Dy^{3+}), $^3H_6$ (Tm^{3+}), $^3F_4$ (Tm^{3+}), $^3H_5$ (Tm^{3+}) and $^3H_4$ (Tm^{3+}). C_{CR} is the CR parameter between a couple of Tm^{3+} ions expressed in cm^3s^{-1}, while K_{TmDy} and K_{DyTm} are the energy transfer parameters respectively from Tm^{3+} ions to Dy^{3+} ions and from Dy^{3+} ions to Tm^{3+} ions. β_{63}, β_{64}, β_{65} are respectively the branching ratios corresponding to the transitions: $Tm^{3+}(^3H_4) \rightarrow Tm^{3+}(^3H_6)$, $Tm^{3+}(^3H_4) \rightarrow Tm^{3+}(^3F_4)$ and $Tm^{3+}(^3H_4) \rightarrow Tm^{3+}(^3H_5)$.

In these calculations, the modeled ridge waveguides present the same geometry as described in the previous section, i.e. a section of 35 × 35 µm² and a 1 cm length. It is considered that a Dy^{3+} population inversion of at least 30% is required to reach enough laser gain, in order to balance the optical losses in the cavity (L=6.5% and T_{oc}=15%) and thus to allow a laser emission at 3.1 µm. The Tm^{3+} spectroscopic parameters in CaF_2 have been calculated using the Judd Ofelt theory [38]. By this way, the radiative lifetimes, branching ratios and the cross relaxation parameters were calculated considering a 5% Tm^{3+} doped CaF_2 sample. The corresponding parameters are the followings: τ_5=10 µs, τ_4=12.33 ms, τ_6=1.71ms, C_{CR}=1.63×10^{-15} cm^3/s, β_{63}=0.884, β_{64}=0.08, β_{65}=0.036.

The ET coefficient (K_{TmDy}) from the $^3F_4$ (Tm^{3+}) level to the $^6H_{13/2}$ (Dy^{3+}) upper laser level has been determined in the previous section to be equal to 3.38 ×10^{-17} cm^3.s^{-1}. Furthermore, it has been considered that no energy back-transfer from Dy^{3+} to Tm^{3+} ions occurs (K_{DyTm} = 0 cm^{3}s^{-1}), neither upconversion processes among excited Dy^{3+} ions (K_{uc}(Dy) = 0). The absorption cross-section σ_{abs} of Tm^{3+} ions in CaF_2 at 767 nm is equal to 4.7 ×10^{-21} cm², which is large enough to absorb entirely the pump energy along 1 cm. The laser performance of codoped Tm^{3+}-Dy^{3+}:CaF_2 waveguides pumped at 767 nm have been compared for various doping ratios of Dy^{3+} ions (i.e: 0.5%-1%-2 %), while the Tm^{3+} concentration has been set to 5%.

Knowing that the evolution of the pump intensity along the propagating z axis follows Eq.8:

$$I_p(z+dz) = I_p(z) - \left(\sigma_{abs}^{P} N_3 dz\right).I_p(z) \qquad \text{(Eq.8)}$$

The numerical model leads to P_{out}^{model} as a function of incident pump power and thus to the laser threshold P_{thr}^{model} (W), as well as to the laser efficiency η^{model} according to Eq.6f.

These modeling results are presented in figure 12, which represents the output power of the laser emission at 3.1 µm versus the Dy^{3+} concentrations, for various incident pump power P_{inc}, which have been set to 1 W, 1.5 W and 3 W. Moreover, the influence of the energy transfer coefficient has been also tested, considering in one hand the energy transfer coefficient that has been obtained from the spectroscopic study ($K_{Tm\text{-}Dy}$ = 3.38 ×10^{-17} cm^3.s^{-1}) and in another hand by considering an excellent energy transfer (i.e. $K^*_{Tm\text{-}Dy}$ = 500 × $K_{Tm\text{-}Dy}$).

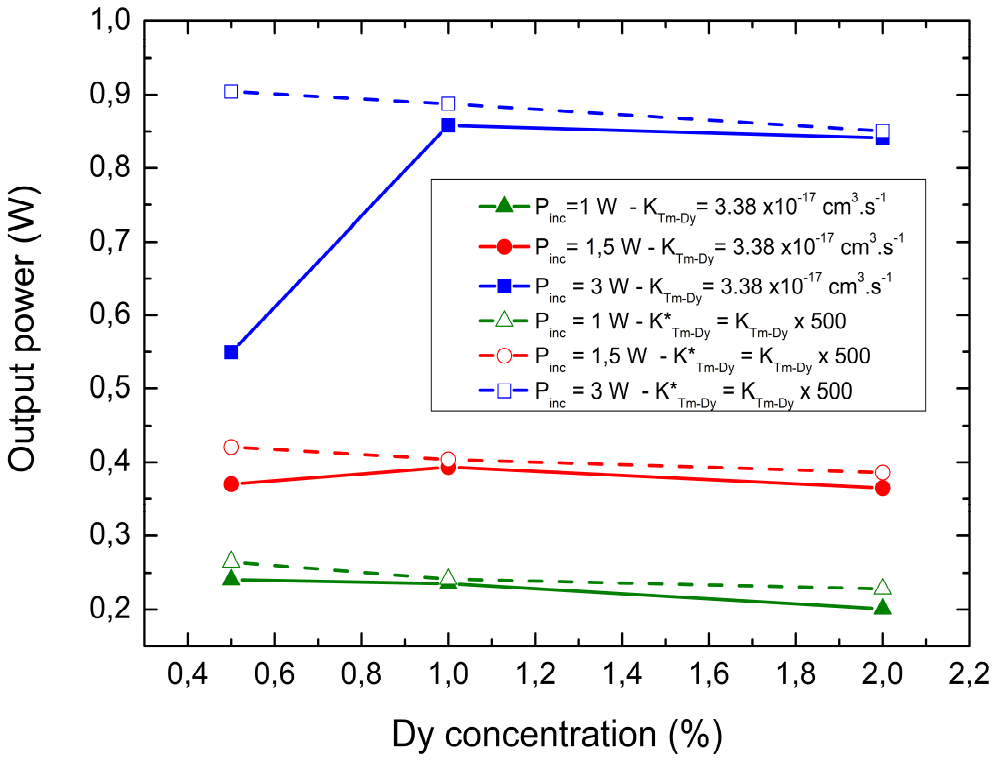

Figure 12: Modeled output powers at 3.1 µm of 5%Tm^{3+}- X%Dy^{3+} doped CaF_2 waveguides, as a function of the Dy^{3+} concentrations (X=0.5 - 1 - 2) for various incident pump powers at 767 nm (P_{inc} = 1W, 1.5W and 3W) and energy transfer coefficients ($K_{Tm\text{-}Dy}$ = 3.38 ×10^{-17} $cm^3.s^{-1}$ and $K^*_{Tm\text{-}Dy}$ = 500 × $K_{Tm\text{-}Dy}$)

Following the same approach as for the singly Dy^{3+} doped systems, it is also possible to give analytical expressions for the theoretical laser threshold and slope efficiency. By considering a very efficient energy transfer from Tm^{3+} to Dy^{3+} ions, which gives two excited Dy^{3+} ions for one excited Tm^{3+} ion in the $^3H_4$ level, the theoretical laser threshold power $P_{thr}^{theoretical}$ and laser efficiency $\eta^{theoretical}$ can be calculated by the following analytical expressions Eq. 9 and Eq. 10:

$$P_{thr}^{theoretical} = \frac{h\nu_P \pi w_p^2}{2.n_{abs}(\sigma_{abs}(\lambda)+\sigma_{em}(\lambda))\tau}\left(\sigma_{abs}(\lambda)N_{Dy}l + \frac{-\mathrm{Ln}(1-T_{OC})-\mathrm{Ln}(1-L)}{2}\right) \text{ (Eq. 9)},$$

$$\eta^{theoretical} = 2\frac{h\nu_L}{h\nu_P} n_{abs} \frac{\mathrm{Ln}(1-T_{OC})}{\mathrm{Ln}(1-T_{OC})+\mathrm{Ln}(1-L)} \text{ (Eq. 10)},$$

One can notice that the two excited Dy^{3+} for one excited Tm^{3+} process appears through the factor 2, for both the laser threshold and slope efficiency. The corresponding theoretical results are reported in table 4.

N_{Dy} (%)	0.5	1	2
P_{thr}^{model}	0.2	0.25	0.35
$\tau(^6H_{13/2})$ (µs)	590	505	475
$P_{thr}^{theoretical}$ (W)	0.17	0.25	0.37
η^{model} (%)	34	34	34
$\eta^{theoretical}$ (%) at the threshold	34.6	34.6	34.6

Table 4: Summary of the numerical modeling and analytical (labelled theoretical) results for 5%Tm^{3+}-X%Dy^{3+}: CaF_2 waveguides, where X = 0.5 – 1 and 2.

The simulated results summarized in table 4 are consistent with an analytical model, where the Tm^{3+} to Dy^{3+} energy transfer efficiency η_{ET} is considered equal to the unity.

In the Tm^{3+}-Dy^{3+} codoped waveguides, the modeled laser thresholds P_{thr}^{model} that have been calculated thanks to the numerical modeling, are lower (Table 4) than in the singly doped Dy^{3+} systems (Table 3) and lie between 0.2 W and 0.35 W. In such cases, the laser efficiency at the threshold is calculated to be ~34%, whatever the Dy^{3+} concentration and an output power in the order of the Watt level is reached by pumping at 767 nm for 3W of incident pump power (Fig.12).

The figure 12 shows a decrease of the output power with respect to the Dy^{3+} concentration when an excellent energy transfer coefficient ($K^*_{tm\text{-}Dy}$) from Tm^{3+} ions to Dy^{3+} ions is considered. This tendency can be perfectly explained by the fact that there is an increase of the laser threshold with the Dy^{3+} concentration, while the laser efficiency at the threshold is remained constant. For Dy^{3+} concentrations higher than 1% and by considering the real $K_{Tm\text{-}Dy}$, this tendency is the same but below this Dy^{3+} concentration, a saturation of the absorption is observed leading to a severe decrease of the output power.

Depending on the considered value of $K_{Tm\text{-}Dy}$, at a Dy^{3+} concentration of 0.5%, the behavior of P_{out}=f([Dy^{3+}]) differs. Indeed, in considering the real value of $K_{Tm\text{-}Dy}$ based on the previous spectroscopic study, the output power is significantly lower than this obtained in considering an excellent energy transfer coefficient ($K^*_{Tm\text{-}Dy}$). By considering the stationary regime, where: $\frac{dN_6}{dt} = 0$, $\frac{dN_5}{dt} = 0$, $\frac{dN_4}{dt} = 0$, $\frac{dN_3}{dt} = 0$, $\frac{dN_2}{dt} = 0$ and $\frac{dN_1}{dt} = 0$, the equations Eq 7a-f lead to:

$$0 = -\frac{N_2}{\tau_2} + K_{TmDy} N_4 N_1 - (\sigma_e N_2 - \sigma_{abs} N_1) I_L \quad \text{(Eq 7.b)}$$

$$K_{TmDy} N_4 N_1 = -\frac{N_4}{\tau_4} + \frac{N_5}{\tau_5} + 2C_{CR} N_3 N_6 + \beta_{64} \frac{N_6}{\tau_6} \quad \text{(Eq 7.d)}$$

$$\frac{N_6}{\tau_6} + C_{CR} N_3 N_6 = \sigma_{abs}^P N_3 I_p \quad \text{(Eq.7f)}$$

Because there is no retrotransfer from Dy^{3+} to Tm^{3+} ions, $K_{DyTm} = 0$; moreover, some simplifications of these equations can be applied to facilitate the understanding of the influence of the considered energy levels, on the involved mechanisms.

In this way, it has been supposed that in Eq 7.d the term $\beta_{64}\frac{N_6}{\tau_6}$ is negligible, as well as the terms $\frac{N_4}{\tau_4}$ and $\frac{N_5}{\tau_5}$; in the same manner, the term $\frac{N_6}{\tau_6}$ is neglected in Eq 7.f. The so obtained simplified equations of Eq 7.d and Eq 7.f lead to:

$$K_{TmDy}N_4N_1 = 2C_{CR}N_3N_6 \qquad \text{(Eq. 8a)}$$

$$C_{CR}N_3N_6 = \sigma_{abs}^{P}N_3I_p \quad \text{(Eq 8.b)}$$

Thus, Eq 7.b becomes:

$$-\frac{N_2}{\tau_2} + 2\sigma_{abs}^{P}N_3I_p - (\sigma_eN_2 - \sigma_{abs}N_1)I_L = 0 \quad \text{(Eq. 8.c)}$$

The equation Eq 8.c shows that in this Tm-Dy codoped system, the Dy^{3+} ions behave like a quasi-3 levels system with an absorption based on Tm^{3+} ions, which presents a quantum efficiency equals to 2. Furthermore, Eq 8.a and Eq 8.b lead to the following expression Eq.8 d:

$$2\sigma_{abs}^{P}N_3I_p = K_{TmDy}N_4N_1 \qquad \text{(Eq. 8.d)}$$

$$\Leftrightarrow \frac{N_4}{N_3} = \frac{1}{N_1} \times \frac{2\sigma_{abs}\cdot I_p}{K_{TmDy}} \quad \text{(Eq. 8.e)}$$

The ratio $\frac{N_4}{N_3}$ allows a quantification of the Tm^{3+} ions absorption saturation. So, it appears clearly that the ratio $\frac{N_4}{N_3}$ increases when N_1 decreases and tends to zero; in other words lower is the Dy^{3+} concentration, lower is the population ratio N_1, leading thus to: $N_4 >> N_3$. By this way, for low Dy^{3+} concentration, i.e 0.5% in this work, there are more Tm^{3+} ions in the $^3F_4$ excited state than on the fundamental $^3H_6$ level, hence the saturation of the absorption. To avoid such a saturation, N_3 should be constant and tends to $N_{tot}(Tm^{3+})$.

The behavior differences of $P_{out}=f([Dy^{3+}])$, at a 0.5% of Dy^{3+} concentration, as a function of the value of K_{TmDy} can also be explained following the same reasoning based on Eq 8.d. A high value of K_{TmDy}, such as K^*_{TmDy}, can be correlated to a value of N_3 which tends to $N_{tot}(Tm^{3+})$, avoiding thus a saturation of the absorption. In another hand, if K_{TmDy} is not high enough, $N_3 << N_{tot}(Tm^{3+})$ and a bottleneck appear on the $^3F_4$ level of Tm^{3+} ions, which deexcite themselves not fast enough: there is a saturation of the absorption, due to an insufficient recycling of the pump energy.

Finally in view of these results, it is reasonable to consider that a 1 cm long Tm^{3+}-Dy^{3+} doped CaF_2 waveguide, with a Dy^{3+} doping level of 1% is enough to get a laser emission at 3.1 µm, when the Tm^{3+} sensitizer concentration is set at 5%. This modeling clearly illustrates the advantages of the Tm^{3+} codoping, which permits a lower Dy^{3+} doping level (~1%) instead of using a strongly singly Dy^{3+} doped CaF_2 crystal (~5%) without saturating the pump absorption. Furthermore, a Dy^{3+}concentration of 1% improves the laser performance in attenuating the parasitic mechanisms, such as concentration quenching that can appear among Dy^{3+} ions. The Tm^{3+} codoping also leads to a reduced quantum defect and a better laser efficiency.

4. Conclusion

After having investigated the spectroscopic properties of Dy^{3+} doped and Tm^{3+}-Dy^{3+} codoped CaF_2 crystals, the latter ones appear to be promising candidates for diode pumped MIR laser systems operating around 3 µm ($^6H_{13/2} \rightarrow {}^6H_{15/2}$ transition). The energy transfer that occurs between excited Tm^{3+} and Dy^{3+} ions is very efficient thanks to the rare-earth clustering effect taking place in CaF_2, which is an obvious asset to allow a favorable population inversion in this three levels laser oscillator. Furthermore, the crystalline nature of CaF_2 presents better thermal properties than glassy materials that could lead to very good laser efficiencies and powerful laser oscillators, especially in a Tm^{3+}-Dy^{3+}: CaF_2 waveguide configuration. Indeed, waveguides present a longer absorption length and a better confinement of the laser modes compared to bulk crystals, allowing thus a higher pump density and a better population inversion to reach the laser threshold. Moreover, the broad absorption and emission bands of Dy^{3+} doped CaF_2 crystals offer the possibility to develop ultra-short pulsed laser sources in the MIR spectral range, which are very attractive for various applications such as medical or LIDAR applications. Following the promising laser results predicted by the model presented in this work, crystalline Dy^{3+} and Tm^{3+}-Dy^{3+} doped CaF_2 waveguides will be fabricated by liquid phase epitaxy in a near future, in order to achieve laser action in these new mid-IR laser devices.

References

[1] M. J. Baker, Júlio Trevisan , Paul Bassan, Rohit Bhargava, Holly J Butler, Konrad M Dorling, Peter R Fielden, Simon W Fogarty, Nigel J Fullwood, Kelly A Heys, Caryn Hughes , Peter Lasch, Pierre L Martin-Hirsch, Blessing Obinaju, Ganesh D Sockalingum , Josep Sulé-Suso, Rebecca J Strong , Michael J Walsh, Bayden R Wood, Peter Gardner, Francis L Martin - **Nature Protocols 9 (8), 1771–1791 (2014)**

[2] V. A. Serebryakov, É. V. Boĭko, N. N. Petrishchev, and A. V. Yan - **Journal of Optical Technology 77(1), 6-17 (2010)**

[3] C. Frayssinous, Vincent Fortin, Jean-Philippe Bérubé, Alex Fraser, Réal Vallée - **Journal of Materials Processing Technology 252, 813-820 (2018)**

[4] H. H. P. Th. Bekman, J. C. van den Heuvel and F. J. M. Van Putten - **Proc. SPIE 5615, 27-38 (2004)**

[5] C.R. Petersen. U. Moller, I. Kubat, B. Zhou, S. Dupont, J. Ramsay, S. Sujecki, N. Abdel-Moneim, Z. Tang, D. Furniss, A. Seddon, O. Bang, **Nature Photonics 8, 830 (2014)**

[6] A. Schliesser, N. Picque and T.W Hansch – **Nature Photonics 6, 440 (2012)**

[7] A-T Le, H. Wei, C. Jin and C-D. Lin **– Journal of Physics B: At. Mol. Opt. Phys. Vol 49, issue 5, 053001 (2016)**

[8] H.J. Worner, J.B. Bertrand ; D.V. Kartashov, P.B. Corkum. D.M. Villeneuve – **Nature, Vol 466, 29 (2010)**

[9] T. Popmintchev, M-C. Chen, D. Popmintchev, P. Arpin, S. Brown, S. Ališauskas, G. Andriukaitis,T. Balčiunas, O.D. Mücke, A. Pugzlys, A. Baltuška, B. Shim,S.E. Schrauth, A. Gaeta, C. Hernández-García, L. Plaja, A. Becker, A. Jaron-Becker, M.M. Murnane, H.C. Kapteyn – **Science Vol 336 (2012)**

[10] B. Wolter, M.G. Pullen, M. Baudisch, M. Sclafani, M. Hemmer, A. sentftleben, C.D. Schröter, J. Ullrich, R. Moshammer, J. Biegert – **Physical review X 5, 021034 (2015)**

[11] L.F Johnson and H.J. Guggenheim, **Appl. Phys. Letters 23, No.2, 96-98 (1973)**

[12] B.M. Antipenko, A. L. Ashkalunin, A. A. Mak, B. V. Sinitsyn, Yu.V. Tomashevich and G.S. Shakhkalamyan, **J. Quantum Electronics 10 (5), 560-563 (1980)**

[13] N. Djeu, V.E. Hartwell, A. A. Kaminskii and A. V. Butashin, **Optics letters 22, No.13, 997-999 (1997)**

[14] M.R. Majewski and S.D. Jackson, **Optics Letters 41, No.10, 2173-2176 (2016)**

[15] Yuen H. Tsang, Atalla. E. El-Taher, Terence. A. King, Stuart. D. Jackson, **Optics Express 14, No. 2, 678-685 (2006)**

[16] R. I. Woodward, M. R. Majewski, G. Bharathan, D. D. Hudson, A. Fuerbach and S. D. Jackson - **Optics Letters 43, No. 7, 1471-1474 (2018)**
[17] M. R. Majewski, R. I. Woodward and Stuart D. Jackson - **Optics Letters 43, No. 5, 971-974 (2018)**
[18] S.D. Jackson – **Applied Physics Letters 83, No. 7, 1316-1318 (2003)**
[19] M.R. Majewski, Robert I. Woodward, Jean-Yves Carree, Samuel Poulain, Marcel Poulain and Stuart D. Jackson - **Optics Letters 43, No. 8, 1926-1929 (2018)**
[20] A. Toncelli, M. Tonelli, A. Cassanho and H. P. Jenssen - **Journal of Luminescence 82, 291-298 (1999)**
[21] P.Y. Tigreat, J-L. Doualan, C. Budasca, R. Moncorgé - **Journal of Luminescence 94–95, 23–27 (2001)**
[22] M.Hu, Y.Wang, Z. Zhu, Z. You, J. Li & C. Tu - **Journal of Luminescence, 207, 226-230 (2019).**
[23] D.N. Papadopoulos, F. Friebel, A. Pellegrina, M. Hanna, P. Camy, J-L. Doualan, R. Moncorgé, P. Georges and F. Druon - Invited in Selected Topics in Quantum Electronics, **IEEE Journal Volume 21, Issue 1 (2015)**
[24] A. Lucca, G. Debourg, M. Jacquemet, F. Druon, F. Balembois and P. Georges – **Optics letters Vol. 29, No. 23 (2004)**
[25] V. Petit, J-L. Doualan, P. Camy, V. Menard and R. Moncorge - **Appl. Phys. B 78, 6, 681-684 (2004)**
[26] R. Soulard, J.L. Doualan,A.Braud, M. Sahli, A. Benayad, G. Brasse, A. Hideur, A. Tyazhev, R. Moncorge, P. Camy - **Optical Materials 72, 578-582 (2017)**
[27] R. Thouroude, A. Tyazhev, A. Hideur, P. Loiko, P. Camy, J-L. Doualan, H. Gilles and M. Laroche - **Optics Letters Vol. 45, issue 16, 4511-4514 (2020)**
[28] V. Petit, P. Camy, J.-L. Doualan, X. Portier and R. Moncorge, **Phys. Rev. B 78, 085131, 1-12 (2008)**
[29] X.Y. Cai, Y. Wang, J.F. Li, Z.J. Zhu, Z.Y. You, Y.J. Sun and C.Y. Tu - **Journal of Luminescence, 225, 117328 (2020)**
[30] J.Heo - **Advanced Solid State Lasers conference (p. LS11), Optical Society of America, January (1997)**
[31] J. Heo, W.Y. Cho and W.J. Chung - **Journal of non-crystalline solids, 212(2-3), 151-156 (1997).**
[32] W. Meng, Y. Xu, H. Guo, C. Lu, C. Hou, M. Lu, P. Wang, W. Li, B. Peng, Y. Lu, W. Wei - **Optical Materials 35, 1499–1503 (2013)**
[33] L. I. Zhongxiu, X. U. Tiefeng, S.H.E.N. Xiang, D.A.I. Shixun, W.A.N.G. Xunsi, N.I.E. Qiuhua and X. Zhang, **Journal of Rare Earths, 29(2), 105-108 (2011)**
[34] Y. Tian, R. Xu, L. Hu, J. Zhang, **Materials Letter 69, 72–75 (2012)**
[35] H. Zhao, S. Jia, X. Wang, R. Wang, X. Lu, Y. Fan, M. Tokurakawa, G. Brambilla, S. Wang, P.Wang - **Journal of Alloys and Compounds, 817, 152754 (2020)**.
[36] P. Loiko, R. Soulard, E. Kifle, L. Guillemot, G. Brasse, A. Benayad, J-L. Doualan, A . Braud, M. Aguilo, F. Diaz, X. Mateos and P. Camy – **Optics Express, Vol. 27, No 9, 12647-12658 (2019)**
[37] L. Gomes, A. Felipe, H. Librantz, and S.D. Jackson - **Journal of Applied Physics 107, 053103, 1-8 (2010)**
[38] B.M. Walsh - ***Advances in Spectroscopy for Lasers and Sensing,*** **403–433, Springer (2007)**
[39] A. Lucca, M. Jacquemet, F. Druon, F. Balembois, P. Georges, P. Camy, J. L. Doualan and R. Moncorgé **– Optics Letters 29, No. 16, 1879-1881 (2004)**
[40] W. Bolanos, F. Starecki, A. Benayad, G. Brasse, V. Ménard, J-L. Doualan, A. Braud, R. Moncorgé and P. Camy - **Optics Letter 37, No. 19, 4032-4034 (2012)**
[41] R. J. Beach, **Optics Communications 123, 385–393 (1996)**

Acknowledgments

The authors acknowledge the French Research National Agency (ANR) through the LabEx EMC3 project FAST-MIR, the ANR project SPLENDID 2, the European Community funds FEDER and the Normandie region, for their financial support and funding.